Modeling Investigation of Liquid Oxygen Flashing Spray with CFD

Meng Luo[1,2]*, Pingping Zhu[2], Usman Rana[1,3], Hu Ma[4], Zhendong Yu[1], Oskar J. Haidn[1]

[1]Faculty of Engineering, Technical University of Munich, Garching, Germany
[2]Beijing Institute of Astronautical Systems Engineering, Beijing, China
[3]Faculty of Engineering, Imperial College London, London, UK
[4]Faculty of Mechanical Engineering, Nanjing University of Science & Technology, Nanjing, China

E-mail: meng.luo@ltf.mw.tum.de

Abstract. Injection of cryogenic propellants (e.g. liquid oxygen) into low-pressure environment (e.g. upper-stage rocket engine) may trigger flashing phenomenon, which severely affects the propellants' mixing and combustion. In order to unveil the characteristics of flashing sprays, numerical models of flashing sprays were developed and validated. First, a developed model based on Adachi-correlation was employed for the flashing spray simulation. The results show good agreements with the experiments, both for the flashing spray morphology and temperature distribution. In the near-injector region, the flashing evaporation dominates the spray vaporization with the evaporation mass flow rate of about 2 orders of magnitude higher than that by the other heat transfers, whereas downstream the injector, the external heat transfer (i.e. heat conduction and convection) does. Furthermore, a new flashing spray model based on the nucleate boiling theory was proposed, which shows an improved agreement of the droplet temperature between the simulation and test data.

1. Introduction

The flashing phenomenon may happen once a liquid is under a sudden depressurization, which results in bubble nucleation, bubble growth, and liquid spray violent atomization and vaporization. This phenomenon benefits some industrial applications, such as paper sheet drying, fuel atomization in internal combustion engines, turbine driving in power plants, seawater desalination [1]. In the aerospace application, however, it may trigger problems to the ignition (e.g. ignition delay or failure) and combustion process (e.g. combustion pressure peak).) of the upper stage rocket engine.

The pioneering research work about the flashing sprays can be traced back to early 1960s. At that time, Brown and York explored water and Freon-11 flashing sprays. The authors noticed that there was a critical superheat for the liquid jet disintegration [2]. Since then a quantity of experimental work has been carried out to further study these sprays [3-6]. As to the modeling, due to the complexity of the non-equilibrium phase change during the flashing, it still remains a great challenge. Based on Adachi-correlation [7], Zuo et al [8] developed a flashing spray model by taking into account of the effect of flashing evaporation and the convection and conduction evaporation. The model was later used and/or improved for the flashing investigation by Raju [9], Schmehl et al. [10], and Ramcke et al. [11]. Nevertheless, some heat transfer (e.g. radiation) and interactions (e.g. momentum exchange)

between the continuous and discrete phases are more or less ignored. In addition, all of these models are based on the Adachi-correlation that is derived for pentane. This correlation should be reconsidered when it was directly employed to the different fluids. Therefore, in the present work, developing proper numerical models by considering the above factors are needed, thus to characterize the LOx flashing spray.

2. Flashing spray model

2.1. Flashing evaporation model

In this section, the flashing evaporation model, proposed by Adachi et al. [7] and Zuo et al. [8], was employed and further improved by considering the heat transfer of radiation and phase interactions (mass, heat and momentum exchange). The flashing evaporation model takes into account of the internal heat transfer by superheated boiling evaporation and the external heat transfer from the surroundings to the droplet.

The internal heat transfer is modeled with Adachi-correlation, as shown below:

$$\dot{m}_{flash} = \frac{\alpha_f A_p (T_p - T_b)}{L(T_b)} \tag{1}$$

$$\alpha_f = \begin{cases} 760(T_p - T_b)^{0.26}, & (0\text{K} \le \Delta T \le 5\text{K}) \\ 27(T_p - T_b)^{2.33}, & (5\text{K} \le \Delta T \le 25\text{K}) \\ 13800(T_p - T_b)^{0.39}, & (\Delta T \ge 25\text{K}) \end{cases} \tag{2}$$

where α_f is the effective internal heat transfer coefficient, T_p, A_p and L(T_b) are droplet temperature, surface area and the latent heat, respectively.

Since the droplets strongly interact with the surrounding gas, the heat transfer by convection and conduction from the surroundings was therefore taken into account. Zuo et al. [8] gave the evaporation rate of a droplet by heat conduction and convection, as shown:

$$\dot{m}_{heat} = 2\pi \frac{\lambda}{c_p} r_0 \frac{Nu^*}{1 + \dot{m}_{flash}/\dot{m}_{heat}} \ln\left[1 + \left(1 + \frac{\dot{m}_{flash}}{\dot{m}_{heat}}\right)\frac{h_\infty - h_b}{L(T_b)}\right] \tag{3}$$

where $\dot{m}_{flash}$ is the evaporated mass flow rate caused by the superheat, $\dot{m}_{heat}$ is the evaporated mass flow rate due to heat conduction and convection, λ is the thermal conductivity, h_b and h_∞ are the enthalpy at the droplet surface and far away from the surface, respectively.

The modified Nusselt number is described as:

$$Nu^* = 2 + \frac{0.552\,\text{Re}_{spe}^{1/2}\,\text{Pr}_{spe}^{1/3}}{(1+\text{B}_\text{T})^{0.7}\,\frac{\ln(1+\text{B}_\text{T})}{\text{B}_\text{T}}} \tag{4}$$

where Re_{spe} is the Reynolds number, Pr_{spe} is the Prandtl number, and B_T is the Spalding heat transfer number.

The transport and thermodynamic properties were evaluated at a temperature using one-third rule suggested by Sparrow and Gregg [12], which is given by:

$$T_{spe} = T_b + \frac{T_\infty - T_b}{3} \tag{5}$$

Due to the high-temperature and low-pressure relative to cryogenic sprays conditions, the ambient radiation is considered, which is shown as

$$\phi_{radi} = \varepsilon\sigma A_p (T_{amb}^4 - T_b^4) \tag{6}$$

$$\dot{m}_{radi} = \frac{\phi_{radi}}{L(T_b)} \tag{7}$$

where ε is the droplet emissivity, and σ is the Stefan–Boltzmann constant.

2.2. Droplet temperature

The droplet temperature can be calculated by the energy balance equation, which is shown as

$$\frac{d\left(c_p m_p T\right)}{dt} = -\dot{m}_{flash} L(T_b) \tag{8}$$

where c_p is the specific heat capacity.

2.3. Droplet trajectory

The droplet trajectory can be determined by the equation as

$$\frac{d\boldsymbol{v}_p}{dt} = \frac{18\mu C_D \,\mathrm{Re}}{24\rho_p d_p^2}\left(\boldsymbol{v}_p - \boldsymbol{v}\right) \tag{9}$$

where μ is the dynamic viscosity and C_D is the drag coefficient.

Since the flash evaporation will thicken the droplet surface boundary layer, which may affect the drag force calculation, a modified drag force model was used by introducing an effective evaporation correlation to the Schiller-Naumann Model [13]. The modified model is described as

$$C_D = \begin{cases} 24\left(1+0.15\,\mathrm{Re}^{0.687}\right)\Big/\left[\mathrm{Re}\left(1+B_M\right)\right], & \mathrm{Re} \le 1000 \\ 0.44\Big/\left(1+B_M\right), & \mathrm{Re} > 1000 \end{cases} \tag{10}$$

where B_M is the Spalding mass transfer number.

2.4. Two-phase interaction

The two-phase interaction is considered by solving the N-S equations of continuous phase with the corresponding source terms, as shown

$$\frac{\partial \rho}{\partial t} + \nabla \cdot \left(\rho \boldsymbol{v}\right) = \varphi_m \tag{11}$$

$$\frac{\partial \left(\rho \boldsymbol{v}\right)}{\partial t} + \nabla \cdot \left(\rho \boldsymbol{v}\boldsymbol{v}\right) = -\nabla p + \nabla \cdot \bar{\bar{\tau}} + \rho \boldsymbol{g} + \boldsymbol{\varphi}_{mom} \tag{12}$$

$$\frac{\partial \left(\rho E\right)}{\partial t} + \nabla \cdot \left(\left(\rho E + p\right)\boldsymbol{v}\right) = \nabla \cdot \left(\lambda \nabla T - \sum h_j \boldsymbol{J}_j + \bar{\bar{\tau}} \cdot \boldsymbol{v}\right) + \varphi_e \tag{13}$$

where φ_m, $\boldsymbol{\varphi}_{mom}$ and φ_e respectively denote the volumetric mass, momentum and heat source, which are calculated in the Lagrange frame for the tracked droplets.

2.5. *Temperature dependent properties*

During the flashing evaporation, the properties of the simulated fluids are highly depended on temperature (see Figure 1). In this study, the fluid's properties are employed with polynomial fitting of the NIST data.

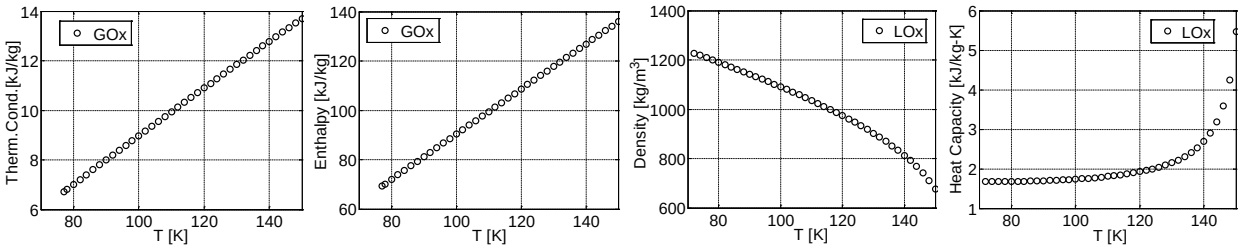

Figure 1. Properties of the simulated fluids.

3. Simulation procedure

3.1. Simulation Setup

In this study, the flashing sprays are simulated with the Euler-Lagrange approach with the FLUENT software. The continuous phase is simulated by solving the U-RANS equations under the Eulerian frame. The discrete phase is tracked by solving the motion equations under the Lagrangian frame. The two-phase are coupled by considering the momentum, energy, and mass exchange.

Since there still lacks proper flashing models in the FLUENT, developed models with User Defined Functions are implemented into the FLUENT solver. Specifically, the "flashing law" and modified drag law are employed to describe the evaporation by flashing and external heat transfer, two-phase heat, momentum and mass exchanges, and droplet trajectory. The fluids' physical and transport properties are described with polynomial interpolation of the NIST database. In the UDFs, when the superheat of the fluids is above zero, the "flashing law" is used; otherwise, the simulation will switch to the common evaporation law (D^2 rule).

Figure 2 gives the simulation mesh, domain and boundary conditions.

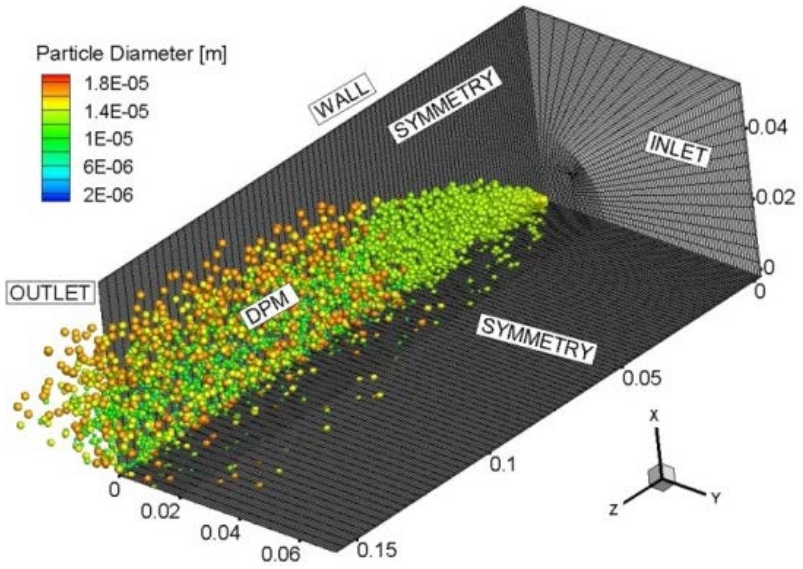

Figure 2. Simulation mesh, domain, and boundary conditions.

A quarter of the chamber domain is used to save the computational cost. As to the continuous phase, the inlet boundary condition is a constant velocity, and the outlet boundary condition is pressure outlet prescribed with the test data. For the discrete phase, the droplet release type conditions uses a solid-cone injection, and the injection velocity, the initial spray angle and the spray mass flow rate are prescribed with the test data. The narrow Roisin-Rammler rule is used to prescribe the initial droplet size distribution.

Computational grid and time step sensitivity studies were performed, which shows that the time step of 1×10^{-5}s with the mesh number of about 180,000 are proper for this study.

Table1 shows boundary conditions of simulation cases.

Table 1. Boundary conditions of the simulation cases

Case	T_{inj}, K	p_c, bar	$\dot{m}$, kg/s	v, m/s	We	D, μm (Rosin-Rammler)			
						d_{max}	d_{min}	d_{mean}	n
#1	111	0.210	9.5×10^{-3}	47	2823	12	8	10	5
#2	116	0.206	7.5×10^{-3}	38	2877	18	10	14	5

4. Results and discussions

4.1. Spray morphological characteristics

Figure 3 displays the experimental and the numerical morphology of the LOx spray under flashing conditions in test case #1. The upper part shows the experimental Schlieren image, and the lower part shows the sumulation result.

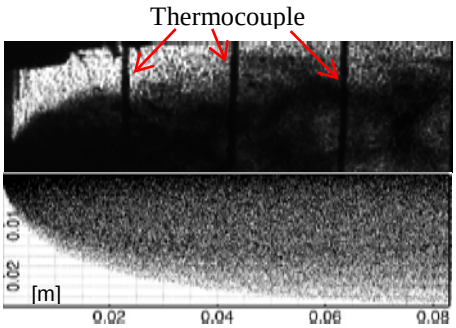

Figure 3. LOx spray contour(bottom:simulation result, top: Schlieren image).

The figure clearly shows a typical flashing phnomonna, i.e. a violent atomization and vaporization with a large bell-shaped spray angle. (notice that the radial width of the spray is about 52mm, while the injetor orifice diameter is only 0.5mm). This violent aotomization and evaporation of LOx is attributed to the massive nucleation and superheted voporization. When the superheted LOx injects into the low pressure chamber enviroment, the liquid clusters with the high internal enegry may overcome the nucleation barrier, which is energy favorable for the bubble nuclei generation. In this case, the bubble nucleation is deemed as a case of heterogeneous since the superheat limit, which happens at about T_{inj}>0.9T_{cri} [14], was not reached. The fast growth and evaporation of the numerous nuclei caused the drastic “explosive” of the liquid jet, leading to flashing sprays.

4.2. Temperature characteristics

Figure 4 illustrates the simulated and test temperature distribution along the LOx spray axial direction. The test data is measured with five thermocouples located along the spray axis with a distance interval of 20mm (see Fig. 3). It shows clearly that the average temperature matches with the test data.

The spray temperature distribution shows a drastic temperature drop near the vicinity of the injector orifice and a gradually decrease downstream the injector as both to the droplets and gas. The gas temperature drops faster than droplet temperature because of the smaller specific heat capacity of the gas phase. Specifically, the droplets’ temperature decreases from about 111K to 84K, which is only 7K above the saturation temperature (T_{sat}=77.4K at 0.21bar), but release almost 80% of its superheat degrees with the droplets just travelling about 20mm (x/d=40) downstream of the spray. This large temperature drop in such a short distance implies a violent heat and mass transfer of the sprays due to the flashing evaporation in this region.

To depict the temperature feature further, the evaporation mass flow rate is analyzed (see Fig. 5). The symbols represent tracked droplets. It can be seen that the spray undergoes a violent flashing evaporation with the evaporation rate of about 10^{-9} kg/s once it released into the low pressure environment, while this evaporation rate experiences a fast drop to about 10^{-11} kg/s just about 20mm downstream the injector. In the same region, however, the evaporation rate by heat transfer of conduction and convection is almost 2 orders of magnitude smaller, with the value of about 10^{-12}~10^{-11} kg/s. Since the ambient temperature is rather low, the evaporation mass flow rate by radiation is even smaller, with the value of about 10^{-13} kg/s. This demonstrates that in the near-injector field, the heat transfer by flashing dominates the spray vaporization than other heat transfers. This overwhelmingly dominated flashing evaporation near the injector leads to the initial drastic temperature drop (see Fig.

4). As a large consume of the superheat of the droplets, the flashing evaporation weakens downstream the injector. On the contrary, the external heat transfer is enhanced due to the increased velocity by evaporation, and when the droplets just traveled about 10mm~20mm, the evaporation rate by external heat transfer is in the same order with the flashing evaporation rate. The total evaporation rate (by both of flashing and external heat transfer) at this point is around 10^{-10} kg/s (one order of magnitude smaller than initial values). As a consequence, the droplet temperature decrease is slowed down. Due to the surrounding gas entrainment, evaporation rate by external heat transfer surpasses the flashing evaporation by about 1 or 2 orders of magnitude downstream the spray. This means the external heat transfer dominate the spray evaporation and results in the gas temperature increase in this region.

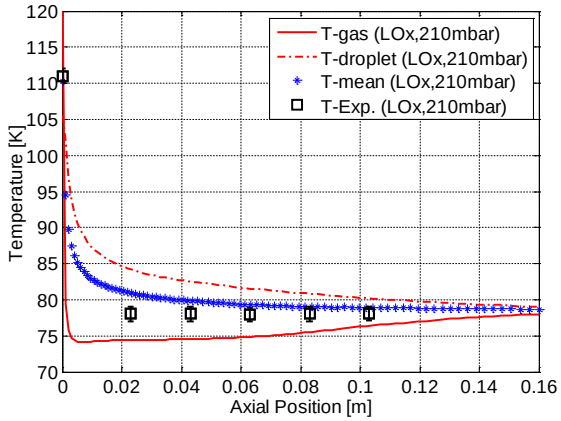

Figure 4. LOx temperature distribution along the spray axis.

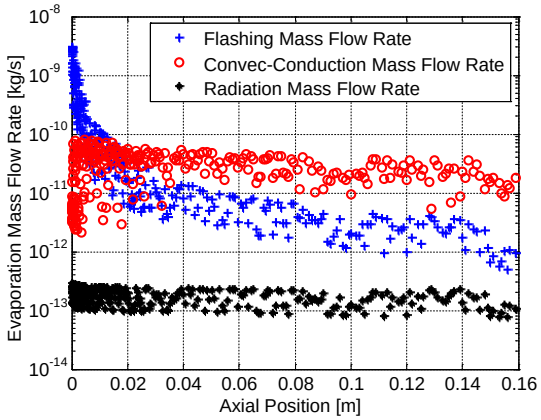

Figure 5. Statistical evaporation mass flow rate.

Remarkably, the simulation results show that, near the injector orifice, the gas temperature drastically drop to about 75K, which is below the saturation temperature of LOx (T_{sat}=77.4K at 0.21bar). The violent flashing evaporation may even lead to the spray temperature drop below the triple point and cause local spray solidification, for example, in our previous test, the solidification of cryogenic droplets (e.g. N_2 and CH_4) were observed [6]. This may have a great threat to the transient start-up of rocket engines.

4.3. Velocity characteristics

Figure 7 shows the LOx droplet velocity fluctuation along the spray radial direction, and it reflects the spray turbulent feature. The normalized velocity Root Mean Square (RMS) is used to describe such turbulent feature, which is defined as:

$$U_{rms} = \sqrt{\frac{u_x'u_x' + u_y'u_y' + u_z'u_z'}{3}} \tag{14}$$

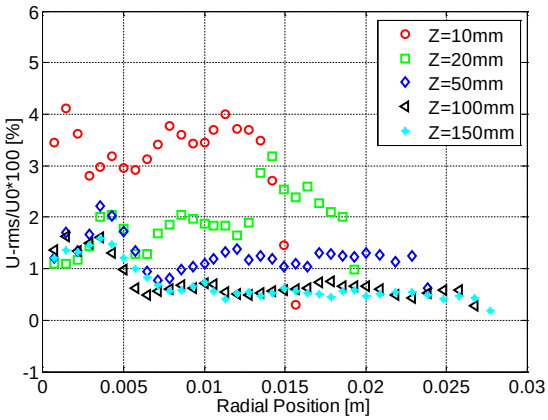

Figure 6. Velocity fluctuation in the spray radial direction.

It can be seen that the normalized RMS profiles present one or two off-axis peaks along the spray radial direction, which indicates a developed shear layer there between the surrounding gas and droplets. The figure shows a large velocity RMS near the injector orifice, whereas the RMS are rather small downstream the injector. For example, the normalized velocity RMS at Z=150 is about 0.5%~1.5%, which is less than half of the value at Z=10mm, which is about 3%~4%. It also shows that the velocity RMS profile presents a large fluctuation near the injector, with a variation of 32%. As the spray develops, however, the velocity RMS distribution turns out to be uniform downstream the injector. These characteristics demonstrate stronger interactions between the droplets and gas at the vincity of the injector, which are mainly attributed to the flashing evaporation in that region.

4.4. Droplet probability distribution

Figure 6 presents the LOx droplet size distribution along the spray centerline. The circular points in the figure are a snapshot of the tacked droplets, and the red solid curve is a statistical average droplet diameter during the simulation. It can be seen that the droplets experience a rapid size reduction once injected into the low pressure environment, and at a short distance of about 30mm, the size decrease contributes to almost 70% of the size reduction in total. Such large size decrease is ascribed to the violent flashing evaporation at the beginning (with an evaporation rate of 10^{-9} kg/s). The scatter curve is fitted, and shows a power-law along the spray axis. Since the initial droplet size is prescribed as the Rosin-Rammler distribution, the droplet sizes in the local Eulerian cell show non-uniform feature.

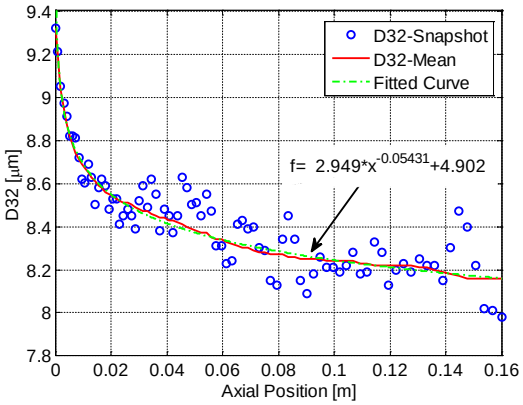

Figure 7. Droplet size distribution in the spray axial direction.

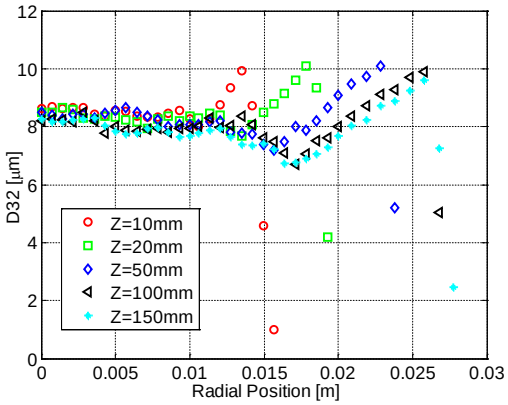

Figure 8. Droplet size distribution in the spray radial direction.

Figure 7 shows the LOx droplet size distribution in the spray radial direction. The figure demonstrates that the droplets' sizes marginally decrease followed by an increasing trend far away from the spray centerline. Such droplet size distribution along the spray radial direction was also obtained by Raju [9] in the simulation work. Due to the small masses and inertial force, the small droplets are supposed to be strongly affected by the surrounding gas. As a consequence, they are entrained towards the spray center by the high velocity gas. Since the large mass and inertial force, the large droplets then move radially outwards of the spray.

4.5. New flashing evaporation correlation

From the above analysis, it can be seen that the developed flashing model reproduce the flashing spray morphology well, and the "average temperature" of droplets and the neighboring vapor is agreement with the test data. However, either droplet or vapor temperature deviates much from the experiments. This deviation might be attributed to the superheat evaporation model (i.e. Adachi-correlation) used. The Adachi-correlation is an empirical correlation derived for pentane (C_5H_{12}), which may not apply well to the cryogenic fluid (e.g. LOx), due to their large differences in properties. Table 2 gives the properties of LOx and pentane. In this section, we developed a new flashing evaporation correlation by considering the fluid properties.

Table 2. Properties of LOx and pentane

Fluids	T_b, K	c_p, kJ/(kg.K)	$L(T_b)$, kJ/kg	σ, mN/m	μ, $\mu Pa.s$	ρ, kg/m^3	λ, mw/(m.K)
LOx	90.1	1.6990	213.18	13.177	195.32	1141.8	150.96
Pentane	308.8	2.3657	357.89	14.282	199.24	610.10	107.41

Since the flashing evaporation is dominated by bubble nucleation and boiling, the droplet evaporation model related to the nucleate boiling is then employed. Under low superheat conditions (e.g. ΔT<5K), the energy provided by the superheat may not enough to support the flashing boiling, but only sufficient to the bubble formation. In this regime, the heat conduction and free convection due to the fluid motion may dominate the evaporation process. The effective internal heat transfer coefficient can be described as [15]:

$$\alpha = 0.15\lambda_l \left[\frac{g\beta\rho_l^2}{\mu_l^2} \mathrm{Pr}_l \right]^{1/3} (\Delta T)^{1/3} \tag{15}$$

where β is the thermal expansion coefficient, ΔT is the superheat degree, λ_l is the thermal conductivity, μ_l is the dynamic viscosity.

Under higher superheat degrees condition (e.g. ΔT>5K), the nucleate boiling becomes increasingly important in the evaporation process. Therefore, the well-known Rohsenow-correlation for the nucleate boiling is employed in this regime, as shown:

$$\alpha = \mu_l L(T_b)\left[\frac{g\left(\rho_l - \rho_g\right)}{\sigma}\right]^{1/2}\left(\frac{c_{p,l}}{C_{s,f} L(T_b)\,\mathrm{Pr}_l^n}\right)^3 \left(\Delta T\right)^2 \tag{16}$$

where $c_{p,l}$ is specific heat capacity, σ is the surface tension, L(Tb) is the latent heat at saturation temperature.

A further simulation work is performed by implementing Eq. (15) and Eq. (16), as a replacement of Adachi-correlation, into the flashing model developed in Section 2.

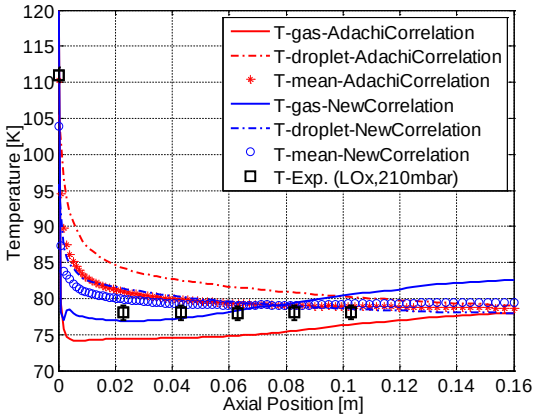

Figure 9. LOx temperature distribution along the spray axis simulated with different flashing evaporation correlations (case #1).

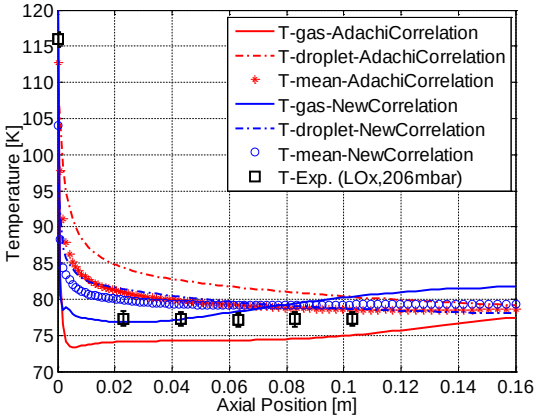

Figure 10. LOx temperature distribution along the spray axis simulated with different flashing evaporation correlations (case #2).

Figure 9 and Figure 10 show the LOx spray temperature distribution simulated with the Adachi-correlation and the new model. It can be seen that the simulated temperature of droplets with the new model matches the experiments better than that with the Adachi-correlation. Notice that the gas temperature, however, shows an increasing trend in the new correlation, which leads to the average temperature deviate more from the test data faraway downstream of the injector. Consider both of the droplets and gas, the results show an improved agreement between the experiments and the simulations in the spray region about x<0.1m. For larger distances from the injector, the data seem to indicate increasing discrepancies (about 4K above the saturation temperature). The slow temperature increase along the spray axis is attributed to the enhancement of external heat transfer by convection and conduction from the surrounding gas, as discussed before.

5. Conclusions

In this paper, a CFD simulation is performed to characterize the flashing spray with the Euler-Lagrange approach. Flashing spray models are developed and implemented into the ANSYS with the consideration of the heat transfer by flashing evaporation, external heat transfer by conduction, convection and radiation, and phase interactions by mass, momentum and heat exchange.

The macroscopic morphology of the LOx flashing spray with a bell-shaped profile is well reproduced, and it matches well with the experiments. The spray temperature distribution is in agreement with the experimental data. The liquid spray experiences a drastic temperature decrease, and releases almost 80% of its superheat near the injector orifice, and afterwards the spray approaches the saturation temperature downstream the nozzle. In the near-injector region (i.e. x/d~40), the heat transfer by flashing is dominated, which is almost 2 orders of magnitude higher than others, while downstream of the sprays, the external heat transfer does. The droplet size distribution shows that smaller droplets accumulate near the spray centerline, and larger droplets locate outwards the spray. A new flashing evaporation model is also developed, which shows an improved agreement between experiments and simulations as to the droplet temperature.

References

[1] Nishimura, Y., Wada, Y., Yamaguchi, A., Yoon, J., Senda, J., and Fujimoto, H., "An experimental study on flash boiling spray using two-component fuel under the condition of advanced injection HCCI", 10th International Conference on Liquid Atomization and Spray, Paper ICLASS06-134, Kyoto, Japan, Sept. 2006.
[2] Brown, R. and L. York, "Sprays formed by flashing liquid jets," AICHE Journal. Vol. 28, No.2, 1962, pp. 149-153.
[3] Shepherd, J. E., and Sturtevant, B., "Rapid evaporation at the superheat limit," Journal of Fluid Mechanics, Vol. 121, 1982, pp. 379-402.
[4] Park, B. S., and Lee, S., "An experimental investigation of the Flash atomization mechanism," Atomization and Sprays, Vol. 4, No. 2, 1994, pp. 159-179.
[5] Lamanna,G., Kamoun., H., Weigand., B., Manfletti, C., Rees, A., Sender, J., Oschwald, M., and Steelant, J., "Flashing behavior of rocket engine propellants," Atomization and Spray, Vol. 25, No. 10, 2015, pp. 837-856.
[6] Luo, M., and Haidn, O. J., "Injection of cryogenic propellants under low pressure conditions," 52nd AIAA/SAE/ASEE Joint Propulsion Conference, AIAA Paper 2016-4790, Salt Lake City, UT, July 2016.
[7] Adachi, M., McDonnel, V. G., Tanaka, D., Senda, J., and Fujimoto, H., "Characterization of fuel vapor concentration inside a flash boiling spray," SAE Technical Paper 970871, Detroit, MI, Feb. 1997.
[8] Zuo, B., Gomes, A. M., and Rutland, C. J., "Modelling superheated fuel sprays and vaporization," International Journal of Engine Research, Vol. 1, No. 4, 2000, pp. 321-336.
[9] Raju, M. S., "CFD modeling of superheated fuel sprays," 47th Aerospace Sciences Meeting including The New Horizons Forum and Aerospace, AIAA Paper 2009-1187, Orlando, FL, Jan. 2009.
[10] Schmehl, R., and Steelant, J. "Flashing-evaporation of oxidizer during start-up of an upper-stage rocket engine," 39th AIAA/ASME SAE/ASEE Joint Propulsion Conference and Exhibit, AIAA Paper 2003-5075, Huntsville, AL, July 2003.
[11] Ramcke, T., Lampmann, A., and Pfitzner, M., "Simulations of injection of liquid oxygen/ gaseous methane under flashing conditions," Journal of Propulsion and Power, Vol. 34, No. 2, 2018, pp. 395-407.
[12] Sparrow, E. M., and Gregg, J. L., "The variable fluid property problem in free convection," Transactions of the ASME, Vol. 80, 1958, pp. 879-886.
[13] Eisenklam, P., Arunachalam, S. A., and Weston, J. A., "Evaporation rates and drag resistance of burning drops," Symposium on Combustion, Vol. 11, No. 1, 1967, pp. 715-728.
[14] Yildiz, D., "Experimental investigation of superheated liquid jet atomization due to flashing phenomena," Ph.D Dissertation, Université Libre de Bruxelles, Belgium, 2005.
[15] Incropera, F. P., DeWitt, D. P., Bergman, T. L. and Lavine, A. S., Principles of Heat and Mass Transfer, 7th ed, John Wiley & Sons, Inc., New Jersey, 2011, Chaps. 10.